Article

Molecular-Based Synthetic Approach to New Group IV Materials for High-Efficiency, Low-Cost Solar Cells and Si-Based Optoelectronics

Yan-Yan Fang, Junqi Xie, John Tolle, Radek Roucka, Vijay R. D'Costa, Andrew V. G. Chizmeshya, Jose Menendez, and John Kouvetakis

J. Am. Chem. Soc., **2008**, 130 (47), 16095-16102 • DOI: 10.1021/ja806636c • Publication Date (Web): 29 October 2008

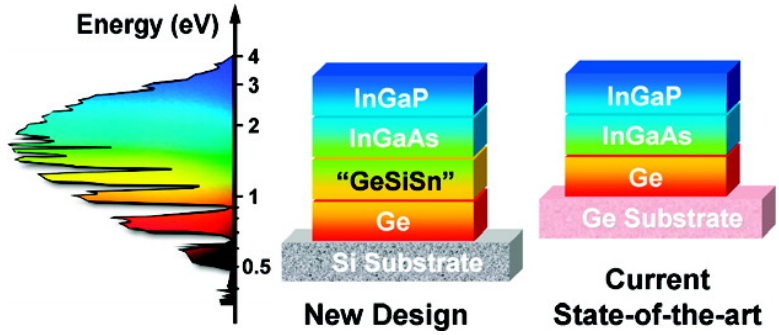

More About This Article

Additional resources and features associated with this article are available within the HTML version:

- Supporting Information
- Access to high resolution figures
- Links to articles and content related to this article
- Copyright permission to reproduce figures and/or text from this article

View the Full Text HTML

J|A|C|S
ARTICLES

Published on Web 10/29/2008

Molecular-Based Synthetic Approach to New Group IV Materials for High-Efficiency, Low-Cost Solar Cells and Si-Based Optoelectronics

Yan-Yan Fang,[†] Junqi Xie,[†] John Tolle,[†] Radek Roucka,[†] Vijay R. D'Costa,[‡] Andrew V. G. Chizmeshya,[†] Jose Menendez,[‡] and John Kouvetakis*,[†]

Department of Chemistry and Biochemistry, Arizona State University, Tempe, Arizona 85287-1604, and Department of Physics, Arizona State University, Tempe, Arizona 85287-1704

Received August 21, 2008; E-mail: Jkouvetakis@asu.edu

Abstract: $Ge_{1-x-y}Si_xSn_y$ alloys have emerged as a new class of highly versatile IR semiconductors offering the potential for independent variation of band structure and lattice dimension, making them the first practical group IV ternary system fully compatible with Si CMOS processing. In this paper we develop and apply new synthetic protocols based on designer molecular hydrides of Si, Ge, and Sn to demonstrate this concept from a synthesis perspective. Variation of the Si/Sn ratio in the ternary leads to an entirely new family of semiconductors exhibiting tunable direct band gaps (E_o) ranging from 0.8 to 1.2 eV at a fixed lattice constant identical to that of Ge, as required for the design of high-efficiency multijunction solar cells based on group IV/III−V hybrids. As a proof-of-concept demonstration, we fabricated lattice-matched Si(100)/Ge/SiGeSn/InGaAs architectures on low-cost Si(100) substrates for the first time. These exhibit the required optical, structural, and thermal properties, thus representing a viable starting point en route to a complete four-junction photovoltaic device. In the context of Si−Ge−Sn optoelectronic applications, we show that $Ge_{1-x-y}Si_xSn_y$ alloys serve as higher-gap barrier layers for the formation of light emitting structures based on $Ge_{1-y}Sn_y$ quantum wells grown on Si.

Introduction

Ternary Si−Ge−Sn semiconductors represent an emerging class of particularly versatile IR materials, since they can be used both as active layers via band gap tuning, as well as enabling structural buffers for the direct integration of dissimilar compounds with silicon.[1−6] They constitute the first practical group IV ternary alloy, since C can only be incorporated in minute amounts into the Ge−Si network to form Si−Ge−C.[7] A wide range of band gaps can be achieved by varying the composition of the SiGeSn alloy. In particular, for a fixed 4:1 Si/Sn ratio, one can obtain a family of compounds lattice matched to pure Ge with variable band gaps covering a wavelength range of interest for photovoltaic applications.

The most efficient solar cells in the market today consist of a stack of lattice-matched layers with nominal compositions $In_{0.49}Ga_{0.51}P/In_{0.01}Ga_{0.99}As$/Ge grown on Ge substrates, as shown schematically in Figure 1 (Note that only a small amount of indium of 1−2 atomic percent is required to lattice match GaAs with Ge). It has been proposed that the efficiency of this configuration can be further increased by incorporating a fourth junction between the Ge cell and the GaAs cell.[8,9] The material in this fourth cell should have a direct band gap E_0 close to 1 eV (between $E_0 = 0.8$ eV for Ge and $E_0 = 1.42$ eV gap for GaAs).[8−10] Unfortunately, the strain-free requirement for this application severely limits the possible materials choices. For example, metastable alloys of $GaAs_{1-x}N_x$ have been proposed as a fourth junction material due to the "giant bowing" effect

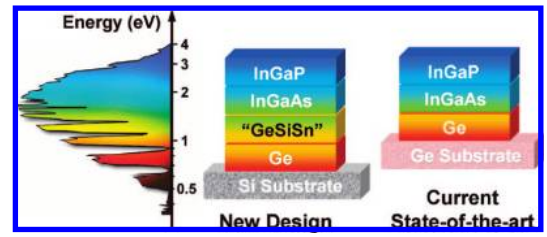

Figure 1. Schematic showing existing (right) and proposed (center) multijunction cell structures based on group IV and III−V hybrid designs. The solar spectrum is shown on the left. In the proposed design, the layer designated "GeSiSn" represents an additional fourth junction comprised of a lattice matched alloy with band gap of 1 eV for improved efficiency.

[†] Department of Chemistry and Biochemistry.
[‡] Department of Physics.

(1) Soref, R. *IEEE J. Sel. Top. Quantum Electron.* **2006**, *12*, 1678.
(2) Sun, G.; Cheng, H. H.; Menendez, J.; Khurgin, J. B.; Soref, R. A. *Appl. Phys. Lett.* **2007**, *90*, 251105/1–251105/3.
(3) Moontragoon, P.; Ikonic, Z.; Harrison, P. *Semicond. Sci. Technol.* **2007**, *22*, 742.
(4) Tolle, J.; Roucka, R.; Chizmeshya, A. V. G.; Kouvetakis, J.; D'Costa, J. R.; Menendez, J. *Appl. Phys. Lett.* **2006**, *88*, 252112.
(5) Kouvetakis, J.; Chizmeshya, A. V. G. *J Mater. Chem.* **2007**, *17*, 1649.
(6) Kouvetakis, J.; Menendez, J.; Chizmeshya, A. V. G. *Annu. Rev. Mater. Res.* **2006**, *36*, 497.
(7) Pantelides, S. T.; Zollner, S. In *Optoelectronic Properties of Semiconductors and SuperLattices*; Manasreh, M. O., Ed.; Taylor & Francis: New York, 2002; Vol. 15, p 538.
(8) Friedman, D. J.; Kurtz, S. R.; Geisz, J. F. *Photovoltaic Specialists Conference: Conference Record of the Twenty-Ninth IEEE* **2002**, 856.
(9) Dimroth, F.; Kurtz, S. *MRS Bull.* **2007**, *32*, 230.
(10) Senft, D. C. *J. Electron. Mater.* **2005**, *34*, 1099.

which induces a rapid reduction in band gap to levels below that of GaAs.[11,12] However, attempts to incorporate such alloys as a solar cell junction have not been successful due to severe materials quality problems. In this regard, the development of our ternary SiGeSn alloys creates a new opportunity in this area, because the lattice constant and the band gap of these materials can in principle be adjusted independently over a wide range spanning the values required for the four-junction designs. Figure 1 compares our proposed high efficiency design concept based on a Si(100)/Ge/SiGeSn/InGaAs/InGaP sequence with the conventional stack. In both cases, the layers in the figure are color-coded to their absorption energies (eV) in accordance with the solar spectrum. Lattice matched Ge/SiGeSn heterostructures of the kind shown here are therefore of particular interest as enabling components in higher efficiency four-junction devices based on group IV/III−V hybrid designs.

Finally, we note that the state-of-the-art Ge/InGaAs/InGaP photovoltaic devices are expensive due to the high cost of the Ge substrate, which represents approximately half to one third of the total cell cost.[13] This limits their applications to the space industry and to sophisticated concentrator architectures. The approach described in this paper offers a straightforward pathway to dramatic cost reductions by replacing the currently used 4−6 in. Ge wafers by thick ($t > 10\ \mu$m) Ge buffers grown on cheap Si(100) platforms (6 in. Ge wafers are approximately 10 times more expensive than the corresponding Si platforms, and this comparison does not take into account other benefits such as the well established and widespread infrastructure associated with the use of silicon processing). Additional cost savings are expected because Si is less brittle and available in even larger sizes, up to 12 in. in diameter. Furthermore, cells fabricated on Si substrates are lighter, which is an important consideration for space applications.

In this paper, we concentrate on the development of synthetic protocols which demonstrate the feasibility of the above concept and closely related optoelectronic designs from a growth perspective. In the latter case, we used previously established synthesis methods to show that SiGeSn alloys can be used as passive barrier layers in light emitting GeSn quantum well structures. For the hybrid multijuntion phovoltaic applications, we show that high-quality SiGeSn alloys containing varying amounts of Si and Sn can be grown reproducibly and reliably on Ge buffered Si(100), for the first time. These are fully relaxed, possess a lattice constant identical to that of Ge, and exhibit tunable direct band gaps ranging from 0.8 to 1.2 eV. The corresponding absorption coefficients can therefore be tuned to match the specific requirements for further improvement in multijunction solar cell devices. Next we produce prototype samples of Si(100)/Ge/SiGeSn substrates on 4 in. wafer formats which are subsequently utilized to grow GaAs and $In_{0.02}Ga_{0.98}As$ with high quality morphological, structural, and optical properties as required for the four-junction structures shown in Figure 1. This successful integration step indicates that the formation of the proposed solar cell architectures is viable and could be extended beyond this proof-of-principle stage. Nevertheless, it should be emphasized that the creation of an actual working device is an exceedingly complicated task involving additional growth and processing steps to form doped structures such as PIN layers of the various junction components. These device fabrication aspects are beyond the scope of the present study.

Results and Discussion

SiGeSn Alloys for Optoelectronic Applications. The preparation of $Ge_{1-x-y}Si_xSn_y$ alloys on Ge buffered Si(100) is conducted by ultrahigh vacuum chemical vapor deposition (UHV-CVD) reactions utilizing SnD_4 as the source of Sn. In prior work, we have shown that these materials can be grown routinely and reproducibly on $Ge_{1-y}Sn_y$-buffered Si(100) using SiH_3GeH_3 and $(GeH_3)_2SiH_2$ as the sources of the Si and Ge atoms.[4,5] The SiH_3GeH_3 compound reacts readily with SnD_4 at low temperatures of 300−350 °C to form Ge-rich compositions with Si and Sn contents spanning from ∼20 to 37% and from 2 to 12%, respectively, depending on the buffer layer lattice dimensions and the deposition conditions, including reaction pressure, temperature, and flow rates.[14,15] This result indicates that the Si concentration range is significantly lower than the 50% value expected from the complete incorporation of the entire Si−Ge (50/50) molecular core of the SiH_3GeH_3 precursor into the film. This is attributed to side reactions in which SiH_3GeH_3 partially dissociates via elimination of stable SiH_4 byproduct. The latter does not react any further, particularly at the low growth temperature employed, leading to the observed lower Si contents in the films. Thus, the thermal dissociation of SiH_3GeH_3 likely proceeds by formation of higher order silygermanes with varying concentrations, including $(GeH_3)_2SiH_2$, according to the reaction described by eq 1:

$$2SiH_3GeH_3 \rightarrow (GeH_3)_2SiH_2 + SiH_4 \quad (1)$$

This latter compound is significantly more reactive and combines readily with SnD_4 to yield films with a Ge/Si ratio of 2:1, precisely matching that of the corresponding precursor. Using this approach, we have been able to grow a host of device-quality samples in which the $Ge_ySn_{1-y}/Ge_{1-x-y}Si_xSn_y$ stack achieves a final strain state that minimizes the bilayer elastic energy, as if the films were effectively decoupled from the substrate. Accordingly, we can produce strained (tensile and compressive) as well as relaxed and lattice-matched $Ge_{1-x-y}Si_xSn_y$ films on suitable Ge_ySn_{1-y} templates. Here we describe the application of this capability to produce light emitting quantum well structures comprised of $Ge_{1-y}Sn_y$ active layers ($E_g < 0.70$ eV) ensconced within higher gap $Ge_{1-x-y}Si_xSn_y$ ternaries ($E_g > 1$ eV) which serve as lattice matched barrier layers in prototype optoelectronic structures. This particular geometry is designed to keep any defects originating from the substrate interface away from the carriers in the $Ge_{1-y}Sn_y$ active material. In addition, the closer proximity of the electron hole pairs increases their recombination rate. Figure 2 illustrates this design experimentally by showing a cros-sectional TEM micrograph of a single SiGeSn/GeSn/SiGeSn quantum well unit. The constituent layers display coherent, chemically abrupt interfaces and a perfectly uniform thickness, as confirmed by atomic resolution imaging using Z-contrast microscopy. This level of microstructural control, normally only achievable by molecular beam epitaxy (MBE), is remarkable in our chemically deposited (CVD) sample. Figure 2 also shows the low temperature (10 K) photoluminescence (PL) signal from the $Ge_{1-y}Sn_y$ quantum wells with composition $y \sim 2.0\%$ Sn as measured by Rutherford backscattering (RBS) and Raman spectroscopy. The PL signal

(11) Wei, S. H.; Zunger, A. *Phys. Rev. Lett.* **1996**, *76*, 664.
(12) Marti, A.; Araujo, G. L. *Sol. Energy Mater. Sol. Cells* **1996**, *43*, 203.
(13) Sherif, R. A.; King, R. R. *Natl. Center Photovoltaics Program Rev. Meet.* **2001**, 261.
(14) Aella, P.; Cook, C.; Tolle, J.; Zollner, S.; Chizmeshya, A. V. G.; Kouvetakis, J. *Appl. Phys. Lett.* **2004**, *84*, 888.
(15) Soref, R.; Kouvetakis, J.; Tolle, J.; Menendez, J.; D'Costa, V. *J. Mater. Res.* **2007**, *22* (12), 3281.

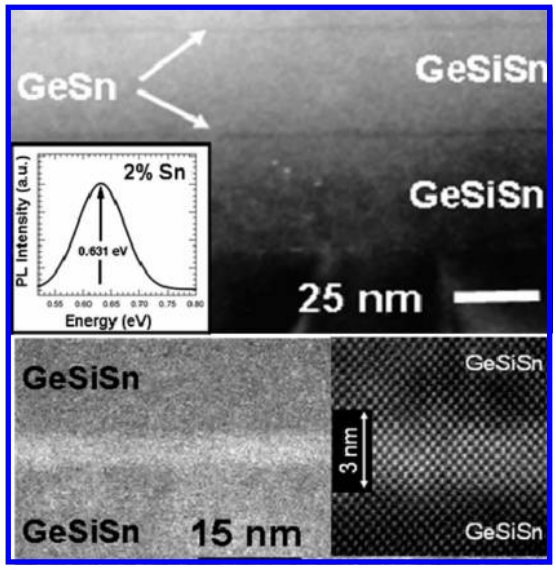

Figure 2. (top) Diffraction contrast XTEM micrograph showing thin $Ge_{0.98}Sn_{0.02}$ quantum wells sandwiched by higher-gap SiGeSn barriers. (inset) PL signal from such a structure. (bottom) Z-contrast image and high resolution micrograph of a single 3 nm thick GeSn quantum well (light contrast).

in this case is relatively weak due to the indirect nature of the band gap and the small sample volume, but it has been confirmed in power dependence studies and is found to be uniform across the sample.

New SiGeSn Alloys for Photovoltaic Applications. Synthesis and Characterization. It should be emphasized that the compositional control in the above application was critical to achieving the desired band gap and fully relaxed strain state which ensured growth of optical quality material. For the photovoltaic design envisioned in Figure 1, the structural and optical requirements for the new $Ge/Ge_{1-x-y}Si_xSn_y$ junctions are achieved by tuning the Si/Sn ratios in the ternary to obtain alloys with lattice constants identical to that of elemental Ge (5.658 Å) and direct gaps in the vicinity of 1 eV. To match the Ge lattice constant, the Sn fraction in the alloy can in principle be increased from zero to a limiting value of ~20%. Here we target a series of intermediate Ge-rich compositions with Sn contents in the range 2−11% that are expected to possess the desired band gaps. The required Si and Sn fractions in these are estimated using a linear interpolation of the Si, Ge, and α-Sn lattice parameters (Vegard's Law).

To produce the required heterostructures, we first deposit enabling Ge buffer layers directly on Si at 350 °C in the nominal thickness range of ~200−750 nm using a newly developed Ge-on-Si CVD method (described elsewhere).[16] These layers exhibit strain relaxed microstructures, extremely low defect densities of $\sim 10^4/cm^2$, and atomically flat surfaces, thus providing an ideal platform for the subsequent formation of the SiGeSn overlayers. The latter films are grown *ex situ* via CVD using a slightly modified synthetic route compared to that previously employed for the analogous SiGeSn-on-GeSn-buffered-Si, which involved binary mixtures of SiH_3GeH_3 and SnD_4.

In the present case, to achieve the higher degree of compositional control required for the lattice matching applications and allow access to a wider range of Si compositions, we have developed an alternative approach based on appropriate stoichiometric mixtures involving $SiH_2(SiH_3)_2$ (trisilane) and/or SiH_3GeH_3 as the silicon source and Ge_2H_6 (digermane). Trisilane contains highly reactive SiH_2 functionalities possessing fewer and far more reactive Si−H bonds, enabling more efficient epitaxy of Si based semiconductors than achievable using the conventional hydrides SiH_4 and Si_2H_6. Our recent studies have established that in general higher order silanes (containing SiH_2 groups) react more readily at low temperatures to form Si at a much higher growth rate compared to Si_2H_6 under the same conditions.[17,18] We note that at temperatures below 450 °C the activation energy of trisilane with respect to H_2 desorption is similar to that of SiH_3GeH_3, indicating that the reactivities of the two compounds are compatible throughout the growth temperature range of interest.[18] Accordingly, we utilize suitable mixtures involving SiH_3GeH_3 and/or $SiH_2(SiH_3)_2$ to obtain Si−Ge−Sn with precisely tuned Si concentrations in the final product for the first time. For example, the synthesis of a typical low Sn concentration end member alloy, $Ge_{0.90}Si_{0.08}Sn_{0.02}$, is conducted via reactions of SnD_4 (as the source of Sn) with $SiH_2(SiH_3)_2$ and commercially available Ge_2H_6 as the sources of Si and Ge, respectively. We find that at the growth temperature of 350 °C pure $SiH_2(SiH_3)_2$ is sufficiently reactive to incorporate the relatively small target levels of Si between 7 and 10%, thus circumventing the need for SiH_3GeH_3, which intrinsically delivers much higher Si contents than required under these conditions. In fact, we have discovered that all of the reactions involving Ge_2H_6 and $SiH_2(SiH_3)_2$ are perfectly stoichiometric and proceed via the following general formula shown by eq 2:

$$x[SiH_2(SiH_3)_2] + y[Ge_2H_6] \rightarrow Si_{3x}Ge_{2y} + (4x + 3y)H_2 \quad (2)$$

This result indicates that $SiH_2(SiH_3)_2$ and Ge_2H_6 react completely via full incorporation of their entire molecular cores to yield compositions $Si_{3x}Ge_{2y}$, reflecting the stoichiometric Ge/Si ratio employed. This mechanism is consistent with our previous studies concerning the thermal activation of trisilane in which it was demonstrated that the unimolecular decomposition of the compound occurs readily at temperatures below 400 °C to deposit pure single crystal silicon films homoepitaxially on (100) surfaces.[19]

As the Sn concentration in the ternary SiGeSn alloy increases to ≥5%, the growth temperature must be reduced in the 330−300 °C to obtain single phase materials with complete Sn substitutionality. In practice, we have found that substitution of Sn in these materials is inversely related to the growth temperature. However, we observe that under these conditions (T < 330 °C) trisilane is comparatively less reactive, resulting in significantly reduced growth rates, which either produced no measurable growth (below 310 °C) or yielded layers which are too thin for device applications but nevertheless sufficient for initial characterization of the alloys. Accordingly, to simultaneously achieve Sn and Si contents higher than 5 and 18% (respectively) in the vicinity required for lattice matching, the use of SiH_3GeH_3 in place of digermane becomes essential and the compound constitutes a source of both Ge and Si. In this regime, a small addition of trisilane to the reaction medium can be used to enhance the Si content and thereby achieve fine-

(16) Fang, Y.-Y.; Tolle, J.; Tice, J.; Chizmeshya, A. V. G.; Kouvetakis, J.; D'Costa, V. R.; Menendez, J. *Chem. Mater.* **2007**, *19* (24), 5910.
(17) Chizmeshya, A. V. G.; Ritter, C. J.; Hu, C.-W.; Tolle, J.; Nieman, R.; Tsong, I. S. T.; Kouvetakis, J. *J. Am. Chem. Soc.* **2006**, *128*, 6919.
(18) Tolle, J.; Chizmeshya, A. V. G.; Fang, Y. Y.; Kouvetakis, J.; D'Costa, V. R.; Hu, C.-W.; Menendez, J.; Tsong, I. S. T. *Appl. Phys. Lett.* **2006**, *89*, 231924.
(19) Fang, Y.-Y.; D'Costa, V. R.; Tolle, J.; Poweleit, C. D.; Kouvetakis, J.; Menendez, J. *Thin Solid Films* **2008**, *516* (23), 8327–8332.

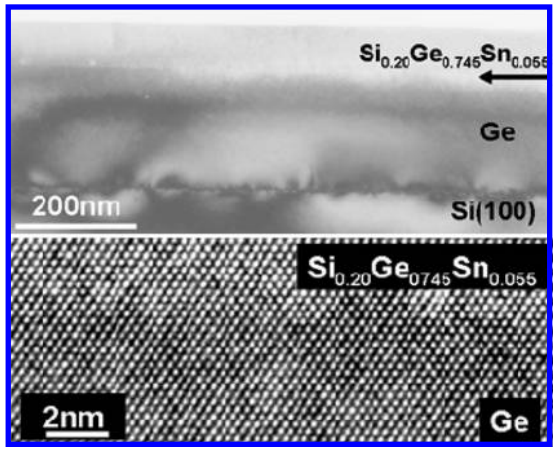

Figure 3. (Top) Bright field XTEM micrograph of the entire Ge/$Ge_{0.745}Si_{0.20}Sn_{0.055}$ film thickness grown directly on Si(100). The arrow in the image indicates the interface between the layers in the heterostructure. (Bottom) High resolution image of the interface showing complete commensuration between the cubic buffer and the epilayer.

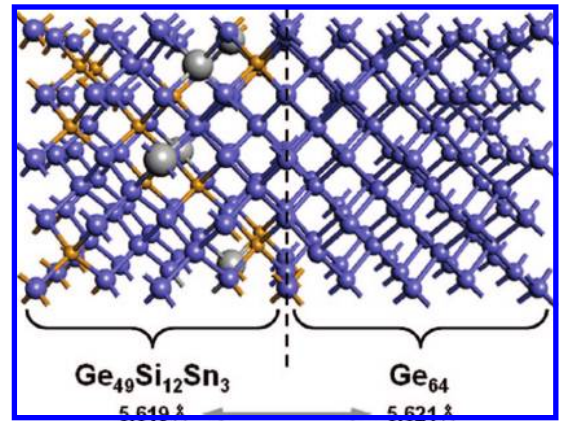

Figure 4. 128-atom (64 × 2) representation of the $Ge_{0.76}Si_{0.19}Sn_{0.05}$/Ge interface obtained from DFT-based first principles structure optimization showing that the lattice matching of this composition with the underlying Ge is readily achievable. Ge, Sn, and Si atoms are represented by blue, gray, and orange spheres, respectively.

tuning of the target composition. The $SiH_3GeH_3/SiH_2(SiH_3)_2$ combination thus provides an unprecedented degree of compositional control and reproducibility, particularly for samples requiring small changes (1−2%) in Si content to achieve exact lattice matching, as we discussed below.

All Si/Ge/GeSiSn materials were characterized by extensive cross-sectional transmission electron microscopy (XTEM), Rutherford backscattering (RBS), atomic force microscopy (AFM), and high resolution X-ray diffraction (HR-XRD) methods, which in general revealed the formation of films with the desired compositions, near perfect microstructure, and a smooth surface morphology. Figure 3 (top) shows a diffraction contrast XTEM micrograph of the entire heterostructure for a representative Ge/$Ge_{0.745}Si_{0.20}Sn_{0.055}$ sample whose Si−Ge−Sn composition lattice matches the underlying Ge buffer. This sample was grown via reactions of SiH_3GeH_3 and SnD_4 at 330 °C at a growth rate of 1.5−2 nm per min to produce a final layer thickness of 80 nm. Note that the 300 nm buffer is devoid of threading dislocations, within the 1 μm field of view shown, and this in turn confers defect-free microstructure and a flat surface morphology onto the 80 nm thick SiGeSn overlayer. The smoothness of the as-grown films is confirmed by AFM scans, which reveal a root mean square (rms) roughness of 1−2 nm for 20 × 20 μm^2 areas depending on the Sn content of the layer. The high resolution image in Figure 3 (bottom) indicates flawless registry across the Ge/SiGeSn interface at the atomic scale, as expected due to the precise lattice matching between the two materials. We note that, under these growth conditions, all reactions of SiH_3GeH_3 and SnD_4 on Ge templates showed a remarkable propensity to reproducibly yield films with approximate stoichiometry in the vicinity of $Ge_{0.75}Si_{0.20}Sn_{0.05}$, in spite of substantial variations in the reactant ratios employed. Our observation suggests that the constituent atoms adopt specific stoichiometries that dimensionally match the underlying Ge substrate via a type of "compositional pinning" mechanism which promotes incorporation of ∼20 atom % Si and ∼5 atom % Sn in the film. To elucidate this behavior, we conducted a first principles DFT study of the Ge/$Ge_{0.75}Si_{0.20}Sn_{0.05}$ interface structure using a $Ge_{64}/Ge_{49}Si_{12}Sn_3$ supercell representation, which corresponds to $Ge_{0.76}Si_{0.19}Sn_{0.05}$, closely matching the experimental structure. All supercell dimensions and atomic positions were simultaneously optimized to yield the ground-state crystalline and electronic structure using the VASP code.[20] The resulting in-plane lattice dimension for the zero-force configuration was found to be 5.620 Å, which corresponds to the average of the individually optimized values of pure Ge (5.621 Å) and the ternary alloy $Ge_{49}Si_{12}Sn_3$ (5.619 Å), indicating that the heterojunction is stress-free. These slightly smaller equilibrium lattice constants obtained in our calculations are due to the well-known shortcoming of the local density approximation (LDA), which typically underestimates bond lengths by ∼1−2%. Note that the Si and Sn atoms in the model shown in Figure 4 were randomly distributed within the SiGeSn portion of the supercell. Models of this kind are currently being used to elucidate the role of interface chemical disorder on the electronic structure (band offsets, optical properties, etc).

Figure 5 shows the electron diffraction data of a 200 nm thick $Ge_{0.90}Si_{0.08}Sn_{0.02}$ alloy (on a 750 nm Ge template) whose band gap and high thermal stability make it a promising candidate for the photovoltaic application described in Figure 1. In this case, the material is grown at 350 °C via reactions of SnD_4 with a mixture of $SiH_2(SiH_3)_2$ and Ge_2H_6 in place of SiH_3GeH_3, which was used in the lower temperature synthesis described above. Note the complete absence of threading defects throughout the entire film within the 1.5 μm × 1 μm field of view in the bright field micrograph (Figure 5 top). High resolution images in (110) projection indicate perfect heteroepitaxy, and selected area electron diffraction (SAED) patterns reveal a complete coincidence of the Ge and $Ge_{0.90}Si_{0.08}Sn_{0.02}$ reciprocal lattice spots, indicating that the corresponding cell dimensions are identical (Figure 5 bottom).

The RBS analysis of the various samples produced in the study corroborated the XTEM observed thickness and also determined the Si, Sn, and Ge concentrations. Ion channeling confirmed the full substitutionality of the Sn atoms in the Si−Ge lattice and revealed full commensuration between the epilayer and the underlying Si(100). The ratio of the aligned over the random peak heights (χ_{min}) is identical for all three constituent atoms and approaches the 4% limit in bulk Si, indicating a high degree of crystalline perfection in the samples.

HR XRD measurements were performed to confirm lattice matching, determine the precise in-plane and vertical unit cell parameters, and study the temperature dependence of the

(20) Kress, G.; Furthmuller, *J. Phys. Rev. B* **1996**, *54*, 11169.

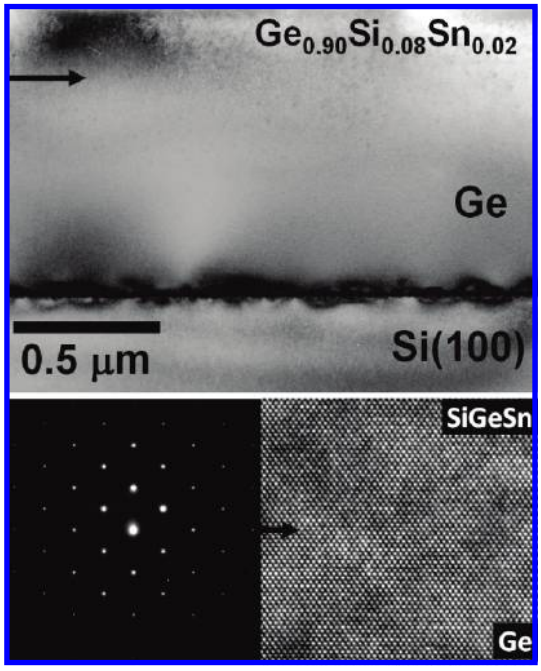

Figure 5. (Top) Bright field micrograph of a Ge/$Ge_{0.90}Si_{0.08}Sn_{0.02}$ film. (Bottom) SAED pattern in (110) projection (left) and high resolution image of the interface (right).

heterostructures dimensions. The $\theta-2\theta$ plots revealed only a single, sharp (004) peak, indicating exact coincidence of the Ge and SiGeSn lattice dimensions. For a typical 400−750 nm thick film, we obtain a (004) rocking curve with fwhm of 200 arcseconds, indicating that the heterostructure is of high crystalline quality. The measured lattice parameters indicated complete absence of any compressive strain and in fact revealed that some of the structures are "over-relaxed", exhibiting a minor tetragonal distortion corresponding to a slight tensile strain as high as 0.12%. For Sn and Si concentrations ranging from 2−11% and 8−42%, respectively, the average room temperature values of the in-plane and vertical lattice parameters of the Ge/SiGeSn heterostructure are $a_0 = 5.664 \pm 0.002$ Å and $c_0 = 5.652 \pm 0.001$ Å.

The XRD data indicated that these lattice matched compositions follow closely Vegard's Law, which assumes a linear interpolation between the lattice parameters of Si, Ge, and α-Sn according to $a_{SiGeSn}(x,y) = (1 - x - y)a_{Ge} + xa_{Si} + ya_{Sn}$, where $a_{Si} = 5.431$ Å, $a_{Ge} = 5.658$ Å, and $a_{Sn} = 6.486$ Å. In our earlier work, we show that the bowing corrections in the Sn_yGe_{1-y} and $Si_{1-x}Ge_x$ systems are positive and negative, respectively, so that their effects essentially cancel in the ternary.[21] As mentioned above, we find in practice that the Si content must be precisely tuned within the range of 1−2% to ensure a close matching of the ternary lattice dimension with that of Ge. For example, high resolution XRD data for the Ge/$Si_{0.075}Sn_{0.020}Ge_{0.905}$ sample yields a relaxed lattice constant of 5.657 Å for both the buffer and the epilayer, in exact agreement with the value 5.657 Å obtained from Vegard's Law above. However, for the Ge/$Si_{0.095}Sn_{0.020}Ge_{0.885}$ sample, which is only slightly richer in silicon, the HR-XRD data reveals a significant splitting in the (004) and (224) peaks, indicating that the epilayer and the Ge buffer are no longer matched, although the nominal Sn content

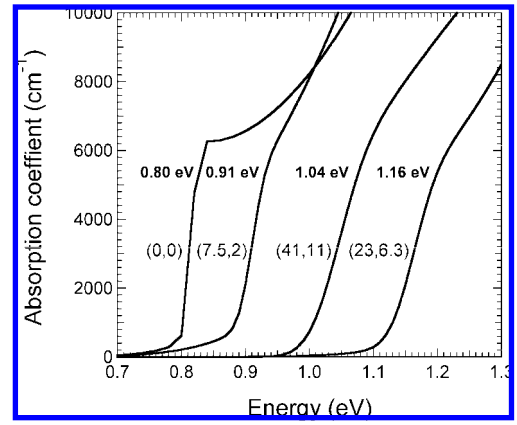

Figure 6. Room temperature absorption coefficient for selected SiGeSn films grown lattice-matched to Ge. The numbers in parentheses next to each curve represent the Si and Sn percentage fraction in each ternary alloy. The data is compared with the absorption coefficient of bulk Ge. The steep increase in absorption corresponds to the lowest direct gap E_0, and we see that this gap can be tuned over a wide range of interest for photovoltaics without changing the lattice parameter. The E_0 values of the materials are shown adjacent to each curve.

in both samples is the same (2%). While both samples were obtained via reactions of Si_3H_8 (trisilane) and Ge_2H_6 (digermane) as shown in eq 1, the $Si_{0.095}Sn_{0.020}Ge_{0.885}$ film was grown using a slightly higher Si_3H_8 concentration. Collectively the data show that the Si/Sn ratios must remain close to 4 for lattice matching to occur, as in the case of $Si_{0.075}Sn_{0.020}Ge_{0.905}$.

Optical Properties. The optical properties of the SiGeSn films were investigated using a variable-angle spectroscopic ellipsometer[22] equipped with a computer-controlled compensator. The samples were modeled as a four-layer system consisting of a Si substrate, a Ge buffer layer, a SiGeSn film, and a surface layer. The ellipsometric data were processed following the methodology described in ref 21. Figure 6 shows the absorption coefficients of selected SiGeSn films lattice-matched to Ge and compares them with pure Ge data. In all cases, the lowest direct gap manifests itself as a sharp rise in the absorption. For Ge, the direct gap is at $E_0 = 0.80$ eV, and we see that it can be increased to above 1.1 eV by adjusting the alloy composition. It is interesting to compare the electronic structure of our ternary alloys with those of conventional binary $Ge_{1-x}Si_x$ alloys. A direct band gap of 1.1 eV corresponds to $Ge_{0.9}Si_{0.1}$, which has a large 0.4% lattice mismatch with Ge. By contrast, our ternary alloys are perfectly lattice-matched to Ge for all values of the band gap. The compositional dependence $E_0(x,y)$ is strongly nonlinear, as can be seen from Figure 6, which indicates that the gap of $Ge_{0.48}Si_{0.41}Sn_{0.11}$ (1.04 eV) is lower than that of $Ge_{0.707}Si_{0.23}Sn_{0.063}$ (1.16 eV). For a simple linear interpolation between the E_0 gaps of Si, Ge, and α-Sn, we would expect the direct gap in Ge-matched alloys to increase monotonically from $E_0 = 0.80$ eV in pure Ge to an extrapolated value $E_0 = 3.1$ eV for the $Si_{0.79}Ge_{0.21}$ alloy. We find that the band gap energy does increase initially as the Ge concentration is decreased, but it reaches a maximum for a Ge concentration $1 - x - y \sim 0.6$ and then it decreases for even smaller Ge concentrations. This can be described by introducing a large negative quadratic contribution proportional to xy. The existence of such large band gap "bowing" is consistent with band structure calculations for

(21) D'Costa, V. R.; Cook, C. S.; Birdwell, A. G.; Littler, C. L.; Canonico, M.; Zollner, S.; Kouvetakis, J.; Menendez, J. *Phys. Rev. B* **2006**, *73*, 125207.

(22) Herzinger, C. M.; Johs, B.; McGahan, W. A.; Woollam, J. A.; Paulson, W. *J. Appl. Phys.* **1998**, *83*, 3323.

$Si_{1-y}Sn_y$ alloys.[18] An in-depth discussion of the compositional dependence $E_0(x,y)$ will be published elsewhere.[23]

The measured E_0 values in Figure 6 overlap the requirements for photovoltaic applications. For the actual design of solar cells based on these materials, additional work will be needed to determine the lowest band gap, which may be lower than E_0 if the system is indirect. Unfortunately, indirect gaps are very difficult to measure with spectroscopic ellipsometry. Using the arguments detailed in ref 21, we estimate that in our alloys the indirect band gap is actually very close to the direct band gap, as is the case in pure Ge.

Thermal Behavior. The application of these films in a practical device context also required a detailed understanding of the thermal response and stability of the structures. Accordingly, we focused on the $Ge_{0.90}Si_{0.08}Sn_{0.02}$ alloy with a band gap close to 0.90 eV. This material is expected to be the most thermally robust because of its relatively low Sn content. The sample was heated *in situ* on the XRD diffractometer to a series of temperatures in the range of 30−700 °C using an Anton Paar high-temperature stage, and the corresponding lattice parameters were recorded at each temperature. The heating was conducted under inert atmosphere conditions in a dynamic flow of UHP nitrogen at a 4 psi overpressure to avoid oxidation or decomposition of the layer. At each temperature, the film was realigned using the Si (224) reflection to correct for any sample drift associated with the diffractometer stage expansion during heating. The lattice parameters of the film were determined from the (224) and (004) reciprocal space maps (RSMs), and the data reveal that the residual strain essentially vanishes at 500 °C ($\varepsilon_{||} = +0.01\%$). In addition, the layers remain lattice matched to Ge from 20−600 °C, as evidenced by the persistent coincidence of the Ge and SiGeSn Bragg reflections.

In Figure 7a, we compare the (224) reflections obtained from the annealed $Ge/Ge_{0.90}Si_{0.08}Sn_{0.02}$ sample at 500, 600, and 700 °C (lower spots) to that recorded at 20 °C for the same sample, as-grown (upper spots). Note that the relaxation line (connecting the plot origin and the substrate Si (224) peak) passes slightly below the center of the 20 °C peaks, indicating the presence of a slight tensile strain in the as-grown film. The 224 plots of the annealed film show that the constituent Ge and $Ge_{0.90}Si_{0.08}Sn_{0.02}$ layers are virtually relaxed and fully lattice matched between 500 and 600 °C, as evidenced by the overlap of the (224) peak maxima and the passing of the relaxation line (arrows) directly through the center of these peaks, respectively. At 700 °C (see third RSM panel), we observe a clear separation of the Ge and $Ge_{0.90}Si_{0.08}Sn_{0.02}$ reciprocal peaks, indicating that the two layers develop a significant mismatch in the vertical direction. The buffer becomes compressively strained with $a = 5.6812$ Å and $c = 5.6878$ Å, as implied by the passing of the relaxation line slightly above center of the (224) Ge peak. The $Ge_{0.90}Si_{0.08}Sn_{0.02}$ overlayer, however, remains cubic ($a = 5.6780$ Å, $c = 5.6781$ Å) and fully relaxed with respect to the substrate (relaxation line passes through the center of the peak).

Prolonged heating of these samples at 700 °C in the XRD stage showed that the $Ge_{0.90}Si_{0.08}Sn_{0.02}$ layer remains cubic and virtually coherent to the underlying Ge layer. This is the expected behavior at higher temperatures (above 600 °C), where the larger coefficient of thermal expansion (CTE) of Ge produces compression in the crystal. In comparison, we note that the presence of a small amount of Si (~8%) in $Ge_{0.90}Si_{0.08}Sn_{0.02}$ slightly lowers the CTE of the alloy. To confirm that the observed decoupling of the Ge and $Ge_{0.90}Si_{0.08}Sn_{0.02}$ layers at 700 °C is due to the inherent thermal mismatch at this temperature, we quenched the sample from 700 °C to ambient and repeated the XRD analysis. The latter revealed a single peak virtually identical to that obtained at 20 °C before annealing, as shown in the right-most panel of Figure 7a. This result indicates that the $Ge/Ge_{0.90}Si_{0.08}Sn_{0.02}$ system follows the expected bulklike thermoelastic response.

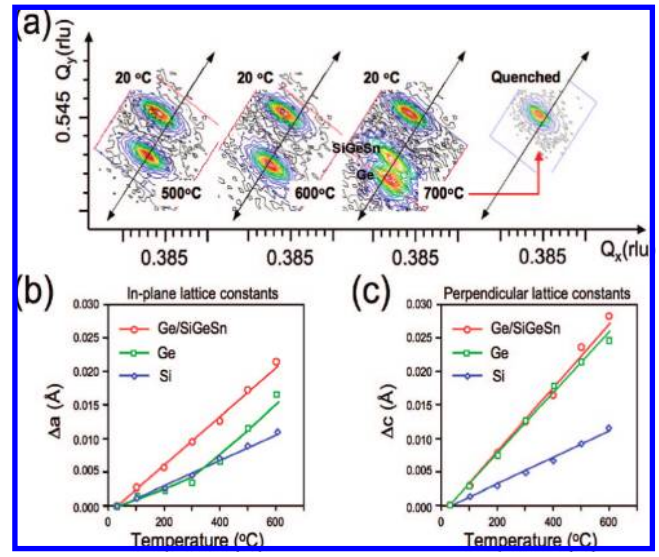

Figure 7. (a) HR-XRD reciprocal space maps of the (224) reflections for a $Ge/Ge_{0.90}Si_{0.08}Sn_{0.02}$ film showing the temperature dependence of the heterostructure upon heating to 700 °C and quenching to ambient. In all panels, the top peaks marked "20 °C" correspond to the room temperature XRD measurement of the film. The lower set of peaks correspond to the annealed $Ge/Ge_{0.90}Si_{0.08}Sn_{0.02}$ sample between 500 and 700 °C. (b and c) In plane and perpendicular (respectively) lattice expansion plots for the $Si(100)/Ge/Ge_{0.90}Si_{0.08}Sn_{0.02}$ sample, the corresponding Ge on Si(100) template, and the Si(100) substrate.

Panels b and c of Figure 7 show plots of the expansion of the in-plane (Δa) and perpendicular (Δc) lattice constants, respectively, for the $Si(100)/Ge/Ge_{0.90}Si_{0.08}Sn_{0.02}$ system (full stack) described in this study (red trace), the corresponding Si(100)/Ge template (green trace), and the Si(100) substrate (blue trace). The data in panel b indicate that the Δa for the Ge layer in the Si(100)/Ge template sample tracks the underlying Si up to 400 °C but expands at the same rate as the $Si(100)/Ge/Ge_{0.90}Si_{0.08}Sn_{0.02}$ layers above this temperature. By contrast, panel c shows that the corresponding Δc of the Si(100)/Ge template matches that of the heterostructure at all temperatures. Collectively, the in-plane and perpendicular lattice dimension data indicate that the films grown on Si(100) are effectively decoupled from the Si(100) over the entire temperature range for $Si(100)/Ge/Ge_{0.90}Si_{0.08}Sn_{0.02}$ and above ~400 °C for the Si(100)/Ge template.

Taken together, these observations indicate that the thermal expansion (CTE) of the Ge and $Ge_{0.90}Si_{0.08}Sn_{0.02}$ layers of the heterostructures is matched up to 600 °C, as shown in Figure 7a. This is an important finding from a practical perspective. First, it is well-known that the CTE of Ge matches that of GaAs, indicating that integration of the classic GaAs/InGaP photovoltaic multijunction on our newly developed $Si(100)/Ge/Ge_{0.90}Si_{0.08}Sn_{0.02}$ group IV platforms can be achieved with minimal thermal stress. Most importantly, this also implies that the $Ge/Ge_{0.90}Si_{0.08}Sn_{0.02}$ structure is perfectly stable under MOCVD growth conditions employed in typical III−V materials process-

(23) D'Costa, V. R.; Fang, Y.-Y.; Tolle, J.; Chizmeshya, A. V. G.; Kouvetakis, J.; Menéndez, J. *Phys. Rev. Lett.*, submitted.

ing (~550−600 °C). In particular, in this temperature range, we find that the $Ge_{0.90}Si_{0.08}Sn_{0.02}$ remains a single phase material with no evidence of Sn segregation or interdiffusion across the interface with the underlying Ge. This indicates that the creation of the first multijunction group IV/III−V hybrid structure (see Figure 1) is feasible from a growth perspective although actual devices will certainly require further refinements in the growth protocols to avoid dopant level migration.

Growth of GaAs and InGaAs on Ge/SiGeSn Platforms. Growth and Characterizations. The prior sections established that the Ge/SiGeSn films grown upon Si are well suited in terms of structure, thermal stability, and optical response to be used in the subsequent growth of the proposed high-efficiency III−V photovoltaic structure. Here we explore the direct growth of the InGaAs component as the next step in the formation of the entire Si(100)/Ge/SiGeSn/InGaAs/InGaP stack. $In_xGa_{1-x}As$ alloys span a wide range of lattice constants and display monotonically decreasing band gaps between those of GaAs (5.65 Å, 1.42 eV) and InAs (6.058 Å, 0.354 eV). In state-of-the-art solar cell applications, $In_xGa_{1-x}As$ layers with to $x \leq 0.02$ have been obtained on both bulk Ge and GaAs substrates. In our own previous work, we have shown that lattice engineered $Ge_{1-y}Sn_y$ buffer layers with concentrations $y = 0.02-0.08$ and lattice parameters between 5.68 and 5.73 Å can be used to successfully fabricate $In_xGa_{1-x}As$ alloys with variable and controllable stoichiometries directly on Si substrates.[24] The latter materials showed much less strain than those grown on conventional substrates such as Ge and GaAs and displayed high quality morphological and structural properties as indicated by their optical properties, which compared well with those measured in fully relaxed micrometer thick layers grown on bulk GaAs. The increased lattice constant of $Ge_{1-y}Sn_y$ relative to the Ge and GaAs makes it possible to form higher indium content $In_xGa_{1-x}As$ with much less strain, leading to improved performance.

A unique feature of the above $Ge_{1-y}Sn_y$ buffer layer approach is that the surface preparation required for subsequent epitaxy of $In_xGa_{1-x}As$ is trivial and straightforward in comparison to that for conventional Ge or Si substrates. In the present solar cell application, the low-Si-content $Si_{0.08}Ge_{0.90}Sn_{0.02}$ surface can also be prepared using a virtually identical chemical cleaning method. *This is an essential enabling step that further demonstrates the viability of the ternary materials as versatile templates for integration of the III−V solar cell components with Si substrates.*

In all deposition experiments, the Si(100)/Ge/SiGeSn substrates were initially cleaned in an acetone/methanol ultrasonic bath, dipped in a dilute HF solution (1%) for 1 min, blow-dried, and then loaded in the growth chamber and outgassed until the pressure reached the base value of $\sim 10^{-8}$ Torr. The reactor is a horizontal low-pressure, cold-wall system fitted with a load-lock and an inductively heated molybdenum block susceptor. A combination of a high capacity turbo pump and a cryo pump is used to achieve UHV conditions, thereby ensuring extremely low levels of background impurities. Prior to deposition, the samples were briefly exposed to a flow of arsine gas (diluted in high purity H_2) at ~500 °C to remove any residual contaminants from their surface. The growth of the $In_xGa_{1-x}As$ layer is conducted immediately thereafter via reactions with $Ga(CH_3)_3$ (trimethylgallium), $In(CH_3)_3$ (trimethylindium), and AsH_3 (arsine). Stock mixtures of $Ga(CH_3)_3$ and AsH_3 with H_2 in 1:10 and 1:15 ratios, respectively, were employed, and their relative concentrations during deposition were regulated by mass flow controllers. The solid $In(CH_3)_3$ compound was dispensed from a glass bubbler using H_2 as a carrier gas, and the specific amount of the material was regulated by its vapor pressure and the H_2 flow rate. A typical deposition was conducted at 550 °C and 50 Torr for 10−15 min, yielding nominal growth rates of 20 nm per min. After growth, the films were slowly cooled to room temperature under a continuous flow of AsH_3 to prevent evaporation of elemental arsenic from the surface layers. Under these conditions, smooth and continuous films were obtained with no evidence of In or Ga metal droplets or surface pits. The samples were thoroughly analyzed by RBS, AFM, XTEM, and HRXRD to determine composition, morphology, microstructure, and crystallographic quality.

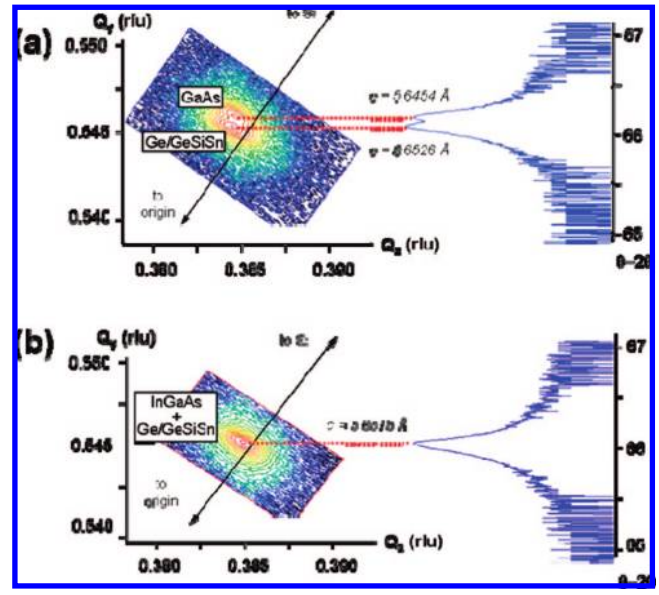

Figure 8. HR-XRD reciprocal space maps (left) and corresponding $\theta-2\theta$ plots (right) of Ge/SiGeSn/GaAs and Ge/SiGeSn/InGaAs samples grown on Si(100). Panel a clearly shows two distinct spots in the (224) RSM associated with the lattice mismatch between the coupled Ge/GeSiSn layers and slightly mismatched GaAs overlayer. The corresponding (224) RSM for the Ge/GeSiSn/InGaAs sample shows only a single spot, indicating perfect lattice matching between the Ge/GeSiSn and InGaAs layers.

Figure 8 shows the high resolution XRD data for a Ge/SiGeSn/InGaAs film grown on Si, and it is compared to a corresponding Ge/SiGeSn/GaAs sample. The latter was prepared during the initial stage of this study for the purpose of establishing optimum growth protocols. The (224) reciprocal space maps show two distinct peaks associated with the Ge/SiGeSn film and GaAs layer, respectively. The SiGeSn lattice dimensions perfectly match those of the underlying Ge layer, and together the Ge/SiGeSn stack imposes a slight tensile strain in the mismatched GaAs overlayer. This is shown in the figure by the position of the line connecting the Si (224) peak with the origin, which passes slightly below the center of the GaAs (224) spot. In contrast, the corresponding RSM plot for the Ge/SiGeSn/InGaAs sample shows only one peak, indicating that the addition of a minor indium content (2 atom %) is sufficient to relieve the strain differential and yield a perfectly lattice-matched Ge/SiGeSn/InGaAs stack, as required for the fabrication of the photovoltaic device. Precise measurements of the lattice constants for the entire stack using the (224) and (004) reflections give $a = 5.660$ Å and $c = 5.6515$ Å, which confirm

(24) Roucka, R.; Tolle, J.; Forrest, B.; Kouvetakis, J.; D'Costa, J. R.; Menendez, J. *J. Appl. Phys.* **2007**, *101*, 013518.

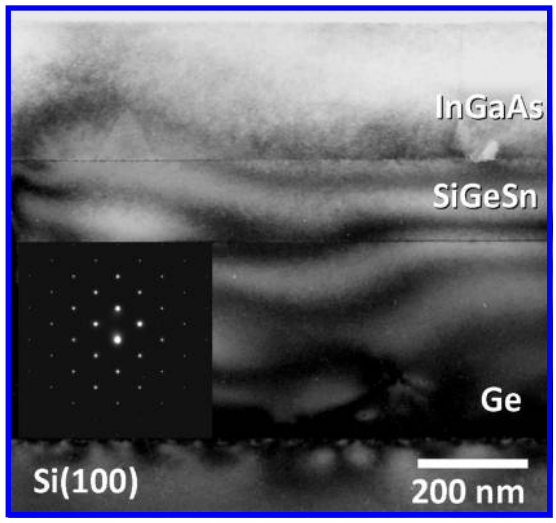

Figure 9. Diffraction contrast XTEM micrograph showing growth of InGaAs on Si(100) via a lattice matched Ge/$Si_{0.08}Ge_{0.90}Sn_{0.02}$ template. The inset is a SAED pattern of the heterostructure in ⟨100⟩ projection showing an overlap of the diffraction spots consistent with the close matching of the lattice dimensions.

that the layers are fully lattice matched and exhibit only a residual tensile strain, which is likely due to the thermal cycling during the fabrication of the stack.

The RBS spectra (not shown) of a typical lattice-matched $In_xGa_{1-x}As$ film grown on Ge/$Ge_{0.90}Si_{0.08}Sn_{0.02}$ comprise of overlapping peaks corresponding to the signals of Ge, Sn, Ga, As, and In. A data fitting procedure using the known buffer layer composition and thickness reveals that the corresponding thickness and stoichiometry of the epilayer are 200−600 nm and $In_{0.02}Ga_{0.98}As$, respectively. The ion channeling spectrum shows a high degree of crystallinity and epitaxial alignment between the various InGaAs, SiGeSn, and Ge components of the film and the underlying Si(100) substrate. The χ_{min} value of the Sn signal is virtually identical before and after InGaAs deposition, indicating that the $Ge_{0.90}Si_{0.08}Sn_{0.02}$ buffer is thermally robust under these processing conditions with the entire Sn content remaining substitutional. Finally, we note that the χ_{min} values for In, Ga, and As in the epilayer are nearly equal (3−6%), indicating that these atoms all occupy equivalent lattice sites in the alloy consistent with single phase material.

AFM studies of both Ge/SiGeSn/GaAs and Ge/SiGeSn/InGaAs samples show a fairly smooth surface with rms values of ∼5 nm. XTEM analysis of these materials reveals single-phase layers in perfect epitaxial alignment. Bright field micrographs of the entire heterostructure and high-resolution images of the epilayer−buffer interface show high quality microstructure and morphology, including sharp, defect-free interfaces and planar surfaces. Occasional dislocations penetrating to the surface are observed in the bright field images. A XTEM micrograph of a representative Si/Ge/$Si_{0.08}Ge_{0.90}Sn_{0.02}$/InGaAs structure showing the entire sequence of the constituent layers is presented in Figure 9. The thicknesses measured here are in close agreement with those determined by RBS.

Summary

In this paper, we demonstrate the fabrication and fundamental viability of new group IV semiconductor materials based on ternary SiGeSn alloys with a potential for disruptive breakthroughs in photovoltaics and silicon photonics. This system provides extraordinary flexibility in optical and structural properties engineering which could be applied to the design and fabrication of novel photonic devices, including multijunction solar cells, high-speed modulators, and multicolor detectors based on SiGeSn/GeSn/Si(100) and SiGeSn/Ge/Si(100) building blocks. In this study, we first demonstrate the formation of SiGeSn/GeSn quantum well stacks in which GeSn active layers are sandwiched between higher gap SiGeSn barriers to produce the first light emitting GeSn structure. Next, we show that SiGeSn alloys (lattice matched to Ge) can be incorporated as the highly sought ∼1 eV gap material to complement the state-of-the-art Ge/InGaAs/InGaP multijunction solar cells, offering the possibility of significant improvement in efficiency and dramatic reductions in device cost. For the latter application, the SiGeSn materials are synthesized for the first time on 4 in. Ge buffered Si(100) via low temperature reactions of Si/Ge/Sn hydrides including SnD_4, SiH_3GeH_3, $SiH_2(SiH_3)_2$, and Ge_2H_6. These compounds enable facile adjustment of the elemental content in the alloy, leading to a wide range of materials that possess a fixed lattice constant identical to that of Ge by maintaining the Si/Sn ratio close to 4:1 in the ternary. For low Sn concentrations ($y \sim 0.02$), the films can be grown at 350 °C using only SnD_4, Ge_2H_6, and Si_3H_6. To obtain higher Sn concentrations, $y \geq 0.05$, the growth temperature must be lowered to 300−330 °C. Under these conditions, the reactivity of trisilane is considerably reduced, and growth of the ternary is achieved using SiH_3GeH_3 as the main source of Si and Ge, with trisilane included as an additive to fine-tune the composition.

The compositional dependence of the E_0 transition was measured for a series Ge/SiGeSn samples with 2−11% Sn using spectroscopic ellipsometry and photoreflectance, yielding tunable absorption coefficients and band gap energies in the range of 0.9−1.2 eV. This observed "decoupling" of band gap and lattice constant is a behavior typical of III−V quaternary compounds that has led to spectacular advances in commodity device fabrication using these materials. However, this is the first time it is observed for group IV elements, which, unlike III−Vs, possess inherent and highly desirable compatibility with Si CMOS processing.

The 0.9−1.2 eV band gaps are higher than that of Ge (0.80 eV), making these materials promising candidates for high efficiency photovoltaic applications. Accordingly, we conducted proof-of-concept MOCVD growth of GaAs and InGaAs films on Ge/SiGeSn templates to demonstrate the viability of the latter in the fabrication of group IV/III−V hybrid solar cell designs. The data indicated that the resultant Si(100)/Ge/SiGeSn/InGaAs heterostructures exhibit the required structural and thermoelastic properties to serve as platforms for the subsequent creation of complete four-junction photovoltaic devices under conditions fully compatible with Si CMOS processing.

Acknowledgment. This work was supported by the US-AFOSR (FA9550-60-01-0442) and the Department of Energy DE-FG36-08GO18003 and the Interconnect Focus Center at Georgia Tech.

JA806636C